IOP Conf. Series: Materials Science and Engineering **418** (2018) 012055 doi:10.1088/1757-899X/418/1/012055

Effect of Temperature and Deformation Speed on Formability of IN718 Sheets: Experimentation and Modelling

K.S. Prasad [a], S.K. Panda [a]*, S.K. Kar [b], S.K. Singh [c], S.V.S.N. Murty [d] and S.C. Sharma [d]

[a] Department of Mechanical Engineering, I.I.T. Kharagpur, Kharagpur, West Bengal, 721302, India
[b] Department of Metallurgical & Materials Engineering, I.I.T. Kharagpur, Kharagpur, West Bengal, 721302, India
[c] Department of Mechanical Engineering, GRIET, Hyderabad, Telangana, 500 072, India
[d]VSSC, Indian Space Research Organisation, Thiruvananthapuram, Kerala, 695022, India

email: sushanta.panda@mech.iitkgp.ernet.in

Abstract. The objective of present work is to get insight into the formability behavior of mill annealed 1mm thick Inconel 718 (IN718) sheets under different elevated temperatures and deformation speeds. The preliminary study consisted of uniaxial tensile testing within a temperature range of 500°C – 700°C at an interval of 50°C and crosshead velocities of 0.03, 0.3, 3, and 30mm/s. It was observed that the total elongation improved by approximately 18% with the increase in temperature from 500°C to 700°C. However, a considerable reduction in total elongation with increase in flow stress was found with the increase in deformation speed at elevated temperatures. Based on the true stress-strain responses, the Johnson-Cook (JC) constitutive equation was developed to capture the material flow behavior. The correlation coefficient (R), average absolute error (Δ) and standard deviation (SDA) were found to be 0.97, 10.8 and 6.8 respectively. Further, stretch forming behavior at isothermal elevated temperatures of 500°C and 650°C were analyzed by performing laboratory scale limiting dome height (LDH) tests. A 20mm width Hasek specimen was deformed at punch speeds of 0.3mm/s and 30mm/s using a sub-sized hemispherical punch of ϕ50 mm. The LDH was found to be higher at 650°C, and the maximum LDH was achieved at lower punch speed of 0.3mm/s. The higher deformation speed decreased the LDH by 7.4% and 12% at 500°C and 650°C respectively. The thermo-mechanical finite element modeling of isothermal LDH tests was developed successfully by incorporating JC model. The predicted punch load, thickness and surface strain distributions were validated with experimental data. It was established that the predicted peak loads were within nominal 8.6% error highlighting the suitability of JC constitutive equation in FE model.

1. Introduction

Inconel 718 (IN718) is a widely used nickel-based superalloy in aerospace industries due to its unique properties such as high strength, oxidation and corrosion resistance even at very high temperatures [1]. Despite these, the poor formability at room temperature in comparison to other aerospace alloys [2,3] limits the widespread application of IN718 in many industries. In this regard, forming at elevated temperature is a promising processing technique and it has been investigated by researchers to improve

the formability with reduced peak loads for many alloys including aluminum, austenitic stainless steel and Ti-4Al-6V [4–6]. However, for designing the optimized process parameter, formability of the material is not only dependant on the temperature alone, but also on deformation speed. It is important to understand the material's flow behavior over a wide range of temperature and deformation speed. In this context, several efforts have been made to understand the deformation behavior of the material through the constitutive models and empirical relations [7].

Finite element (FE) analysis is a critical tool for understanding the complex deformation mechanics that occur during the sheet metal forming process. To accurately analyze the process using numerical methods, the knowledge of material constitutive behavior under severe loading condition is prerequisite. In fact, the accuracy of the numerical models is dependent on how accurately the deformation behavior of the material is being represented by the constitutive model. Recently, several constitutive models have been developed which can be broadly classified into phenomenological models, physical based models and artificial neural networks (ANN) [7]. Physical-based models such as mechanical threshold stress (MTS) and Zerilli-Armstrong (ZA) could provide more accurate results for the deformation behavior over a wide range of temperature and strain rates. However, a large number of material constants and some physical properties may not be readily available in the open literature [6]. ANN is best suited to solve the problems which are difficult to solve by traditional computational methods. The drawback of the ANN is that the model does not offer any physical insight, and model's accuracy depends on the high-quality data [7]. Hence, in the present work, conventional phenomenological based Johnson-Cook (JC) model was used because of its simplicity and less number of constants for easy implementation in the metal forming industries.

The objective of this paper is to understand the deformation behavior of IN718 at elevated temperature domain of $500°C - 700°C$ and deformation speeds of 0.03, 0.3, 3 and 30mm/s. It also aims at developing the JC model using the tensile results and further implementing the developed model into the FE code to predict the formability in terms of maximum punch load, thickness, and surface strain distribution.

2. Materials and Methods

2.1. Uniaxial tensile test

In the present work, mill annealed IN718 sheets of 1mm thickness were used to study the effect of temperature and deformation speed on the formability. In this regard, uniaxial tensile tests and stretch forming experiments were performed on a 50kN servo-electric warm forming machine. Figure 1(a) represents the deformation process sequence of experiments. The samples were placed in the furnace and the heating rate of $10°C/min$ was maintained to reach the desired temperature. Once preferred temperature was attained, the holding time of 900s was maintained throughout the experiments to homogenize the heat across the samples. The deformation was imposed either through pull rod or hemispherical dome punch till the fracture of the specimen. The fractured samples were then furnace cooled and used for further analyses. The inset in Figure 1(a) shows the schematic diagram of tensile test specimen, and the dimensions of the specimen are as per sub-sized ASTM: E8/E8M-11 standards. Figure 1(b) depicts pictorial presentation of the uniaxial tensile test fixture. The test setup consists of lower and upper crosshead where the upper end was fixed and the lower end was movable through which deformation was applied. The experiments were performed at four different initial crosshead velocities of 30, 3, 0.3 and 0.03 mm/s and various isothermal temperatures ranging within $500°C$ to $700°C$ at an interval of $50°C$. The deformation speeds of 30, 3, 0.3 and 0.03 mm/s corresponds to the strain rates of 1, 0.1, 0.01 and $0.001s^{-1}$ respectively. Further, the load-displacement data obtained from various tensile tests were then transformed into true stress (σ) - true strain (ε) data for further analysis.

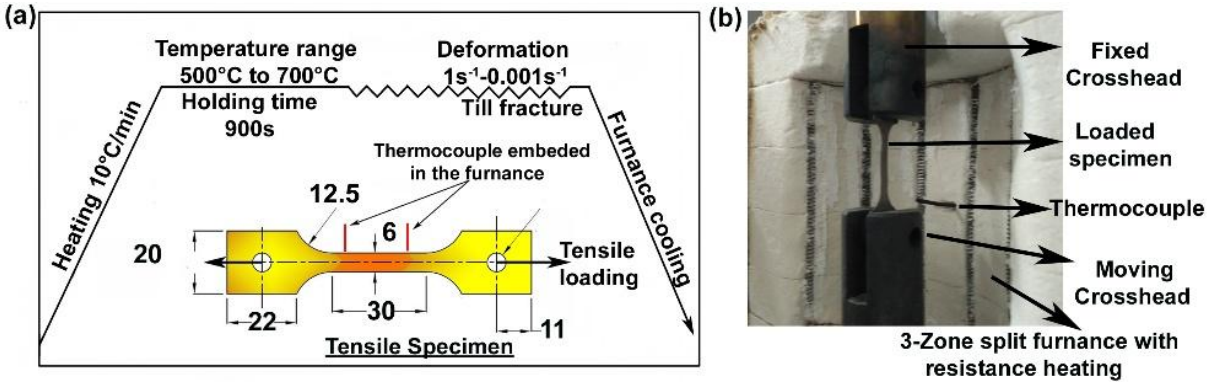

Figure 1. (a) Deformation process sequence and the inset shows the schematic diagram of uniaxial tensile test specimen (b) close view of tensile test setup.

2.2. Limiting dome height test

Stretch forming experiments at elevated temperatures and different punch speed were carried out using a laboratory scale LDH setup as shown in Figure 2(a). The fixture consist of lower die, upper die, and hemispherical punch of 50mm diameter. Both die and pull rods were made of nickel base IN625 superalloy to avoid the erroneous results while performing tests at elevated temperature. Hasek shaped blanks [1] of 150mm length with 20mm width were used to evaluate the stretch forming behavior at isothermal elevated temperatures of 500°C and 650°C. In order to restrict the material flow into the die cavity, the circular groove of lock bead at a diameter of 130 mm was provided in the lower die and the boss of the lock bead at the corresponding location was provided in the upper die. Prior to deformation, circular grids of 2.5 mm diameter were electrochemically etched on the surface of blanks to evaluate the surface strains of the deformed blank. The blanks were stretched with the progression of punch movement, and the test was immediately stopped when load dropped to 90% of maximum load. All the stretch forming experiments were carried out under dry condition without using any lubricants. After deformation, circular grid analysis [8] was carried out to evaluate the strain distribution across the longitudinal direction of the specimen.

3. Constitutive model

In the present work, the JC model was used to describe the deformation behavior of the material as shown in Equation (1). The first, second, and third terms in the parenthesis of Equation (1) refer to isotropic hardening, strain rate hardening and thermal softening respectively. The model considers all these three phenomena independently and their total effect is obtained by multiplying them [9].

$$\sigma=\left(A+B\varepsilon^{n}\right)\left(1+C\ ln\ \dot{\varepsilon}^{*}\right)\left(1-T^{*m}\right) \tag{1}$$

Where, σ, B, n, and ε represents flow stress, strength coefficient, strain hardening exponent, and plastic strain respectively. The constant 'A' stands for yield stress at reference strain rate ($\dot{\boldsymbol{\varepsilon}}_{\mathbf{0}}$) and reference temperature (T_r). The term $\dot{\varepsilon}^{*}$ represents dimensionless strain rate (where $\dot{\varepsilon}^{*} = {}^{\dot{\varepsilon}}/_{\dot{\varepsilon}_0}$ and $\dot{\varepsilon}$ denotes strain rate) and T^{*} stands for dimensionless normalised temperature with respect to reference temperature T_r (i.e. $T^{*} = \frac{T-T_r}{T_m-T_r}$ where T is absolute temperature and T_m as melting temperature). For the present work, the value of T_m, T_r and $\dot{\varepsilon}_0$ were considered to be 1930°C, 500°C, and 1s^{-1} respectively. The material constants C and m represents the coefficient of strain rate hardening and thermal softening exponent respectively. At T= T_r, there is no thermal softening term and the Equation (1) reduces to $\sigma=\left(A+B\varepsilon^{n}\right)\left(1+C\ ln\ \dot{\varepsilon}^{*}\right)$. Further, $\left(\frac{\sigma}{\left(A+B\varepsilon^{n}\right)}-1\right)$ vs. $ln\ \dot{\varepsilon}^{*}$ was plotted for

every strain value at various strain rates. Hence, twenty different values of *C* were obtained from the slopes of the plots. In similar manner, at $\dot{\varepsilon} = \dot{\varepsilon_0}$, the strain rate hardening term was eliminated and this resulted in twenty values of *m*. All total twenty values of C and m were obtained, and the optimum values of *C* and *m* were estimated using constrained optimization technique (Equation (2)).

$$\Delta = \frac{1}{N}\sum_{i=1}^{i=N}\left|\frac{\sigma^i{}_{\exp}-\sigma^i{}_{\mathrm{p}}}{\sigma^i{}_{\exp}}\right| \times 100. \tag{2}$$

Where, Δ is the average absolute error between the experimental ($\sigma_{\exp}$) and predicted flow stress (σ_{p}) and *N* is the total number of data points being considered. The predictability of the constitutive equation was also quantified by employing standard statistical parameters such as correlation coefficient (R). It is mathematically expressed as

$$R = \frac{\sum_{i=1}^{i=N}(\sigma^i{}_{\exp}-\bar{\sigma}_{\exp})(\sigma^i{}_{\mathrm{p}}-\bar{\sigma}_{\mathrm{p}})}{\sqrt{\sum_{i=1}^{i=N}(\sigma^i{}_{\exp}-\bar{\sigma}_{\exp})^2 \sum_{i=1}^{i=N}(\sigma^i{}_{\mathrm{p}}-\bar{\sigma}_{\mathrm{p}})^2}} \tag{3}$$

where $\bar{\sigma}_{\exp}$ and $\bar{\sigma}_{\mathrm{p}}$ are the average values of $\sigma_{\exp}$ and σ_{p} respectively. It is not necessary that the performance of the model is high if the value of R is high, as the model might have a tendency to be biased towards higher values or lower values of the data. Hence, Δ and standard deviations (SDA) were evaluated as an unbiased statistics for measuring the predictability of the model. The detailed formulation for evaluating material constants of JC model are mentioned elsewhere [9].

4. Coupled thermo-mechanical finite element model

Finite element model of the stretch forming process was developed as shown in Figure 2(b). The simulations were carried out using commercially available dynamic-explicit LS-DYNA software. The tools such as punch, die, and binder was considered to be rigid body whereas the blank was considered to be a deformable body. The flow behavior of the blank was defined by the developed JC model and it was implemented in FE codes. The blank was meshed using four-node Belytschko-Tsay shell elements with five integration points.

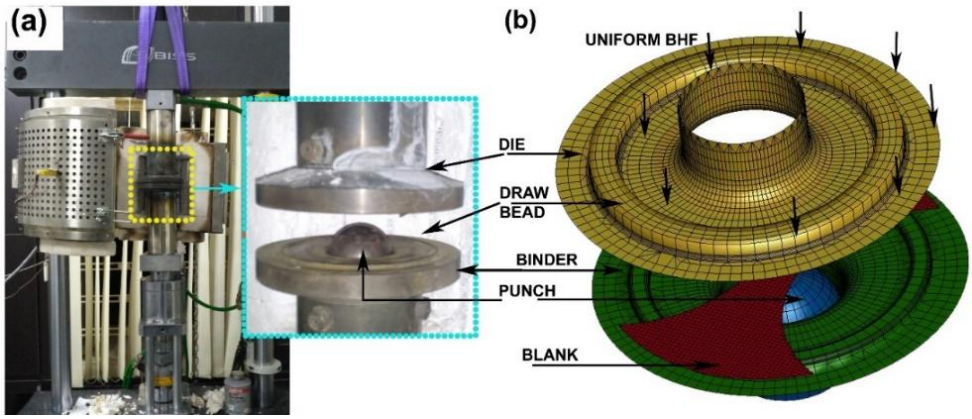

Figure 2. (a) Experimental stretch forming setup, (b) numerical FE model.

The surface contact provides a way of interaction between slave (tools) and master (blank), and for the present work *contact one way surface to surface card* was adopted. A constant coefficient of friction between the tool and blank was used, and the values were defined to be in the range of 0.3-0.5 as per the temperature considered [10,11]. The tools and blank were modeled with a built-in isotropic thermal material model, and thermal properties used are shown in Table 1. The explicit dynamic simulation requires finite small steps which result in high computation time. Hence, to reduce the solving time, the

actual simulations were carried out at deformation speed of 1000mm/s [15]. Subsequently, the rate and temperature dependent parameters, such as strain rate and thermal conductivity were scaled [4].

Table 1: Thermal properties of tool and blank used in the numerical analysis [12–14]

Material	Thermal density (kg/m^3)	Heat capacity (J/kg K)	Thermal conductivity (J/m K)
Tool (IN625)	8440	410	13.4(500°C), 14.6 (650°C)
Blank(IN718)	8190	435	19.1(500°C), 21.2(650°C)

5. Results and Discussion

5.1. Effect of strain rate and temperature on the tensile behavior

The true stress-strain curves evaluated from the tensile tests at different elevated temperatures for the strain rates ranging from quasi-static ($0.001s^{-1}$) to dynamic ($1s^{-1}$) conditions are shown in Figure 3. It was observed that the total elongation improved by approximately 18% with the increase in temperature from 500°C to 700°C. However, a considerable reduction in total elongation with increase in flow stress was found with the increase in deformation speed at elevated temperatures. The improvement in total elongation was found to be highest at 650°C under the lowest strain rate of $0.001s^{-1}$. Moreover, at 650°C, the total elongation was found to improve tremendously by approximately 65.4% and 16.5% in comparison to that of the room temperature [1] and 500°C respectively.

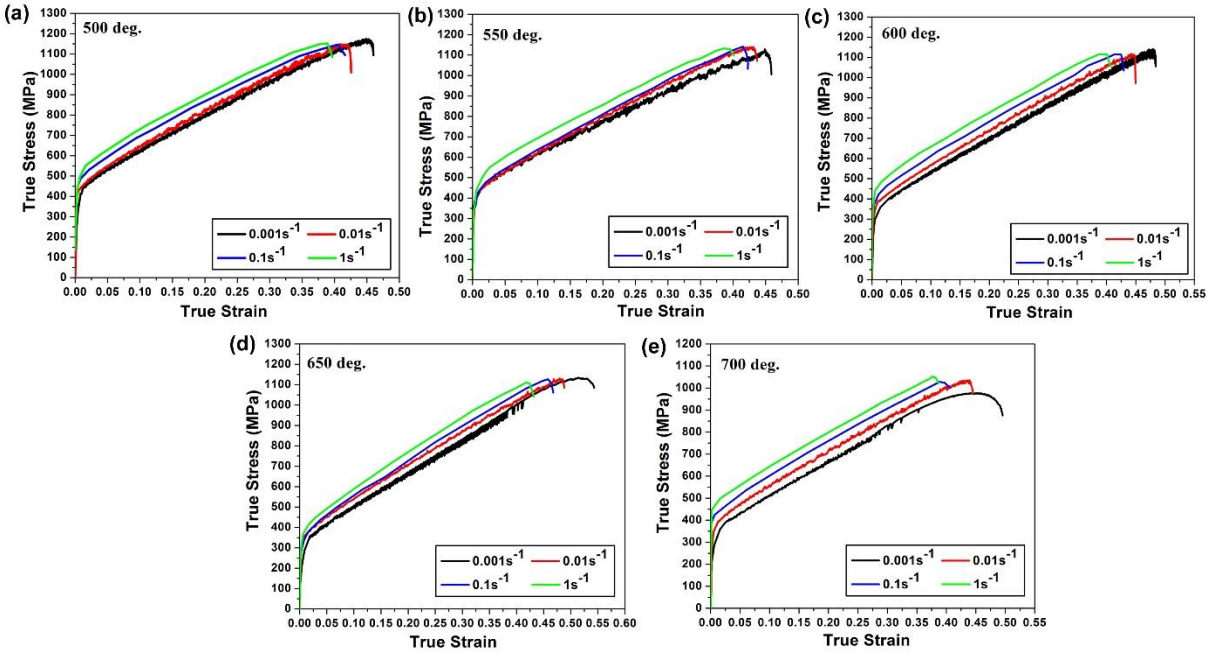

Figure 3. True stress-strain curves obtained at (a) 500°C, (b) 550°C, (c) 600°C, (d) 650°C, and (e) 700°C for the strain rates of 0.001, 0.01, 0.1, and $1s^{-1}$.

Also, with an increase in deformation duration i.e. at lower strain rates, the evolution of precipitates are certain [6]. Hence, the visible jerky stress-strain response can be observed for all the temperature states with $0.01s^{-1}$ and $0.001s^{-1}$ strain rates. The serrations appear when the solute atoms are able to diffuse at a faster rate than the speed of the dislocations to catch and lock them. Therefore, the locked dislocations increase the load and there is a sudden load drop when the dislocations overcome these solute atoms with an increase in plastic strain. This process occurs many times causing serration in the stress-strain curve. This serrated flow is often referred as dynamic strain aging (DSA) phenomenon. Based on the experimental results, the stress data were taken at strain intervals of approximately 0.02 to evaluate the material constants of the constitutive model.

5.2. Adequacy of Johnson-Cook Model

Figure 4(a) shows the predicted versus experimental flow stress. The prediction capability of constitutive model was assessed by three statistical parameters viz. correlation coefficient (R), average absolute error (Δ), and standard deviation (SDA). It was observed that the model could predict the flow behavior very well with R of 0.97, and the corresponding Δ and SDA values were 10.8% and 6.8% respectively. The material constants of JC model evaluated after the optimized technique are also shown in the inset of the figure. The predicted true stress-strain curves at selected strain rate and temperature combination are depicted in the Figure 4(b). It can be inferred from the graph that the prediction under reference strain rate ($1s^{-1}$) and reference temperature ($500°C$) was perfectly matching with the experimental data. Moreover, the deviation from the experimental data seemed to increase with an increase in temperature and plastic strain. It is clearly evident from the figure that the maximum deviation of approximately 140-150MPa was observed at $650°C$ and the deviance was more prominent towards the higher plastic strains regime of 0.28-0.38. This is due to fact that the JC model considers thermal softening, strain rate hardening, and strain hardening as three dependent phenomenon, which increases the error in predicted flow stress as we move away from reference temperature and reference strain rate.

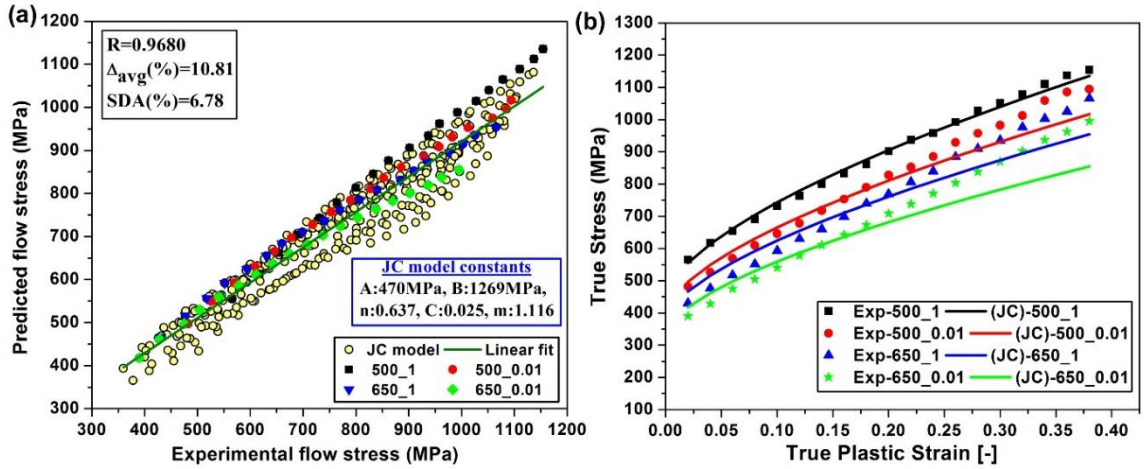

Figure 4. (a) Predictability of JC model, (b) experimental vs. predicted true stress-strain curve.

5.3. Validation of developed constitutive model

In order to validate the developed model, stretch forming simulation at a selected temperature and punch speed (mentioned in Figure 4(b)) were carried out. The results at a particular time step were considered where the simulated cup attains the experimental dome height as shown in Figure 5(a). It can be observed that model could able to capture the maximum thinning at the same location. The experimentally obtained LDH value at different forming conditions is depicted in Figure 5(b). It is interesting to note that with an increase in temperature from $500°C$ to $650°C$ the LDH value was found to increase by 12% when the punch velocity was 30mm/sec and the value increased to 13.6% when deformation speed was 0.3mm/sec. The highest LDH was achieved at $650°C$ with deformation speed of 0.3mm/sec which is in agreement with the uniaxial tensile results (Figure 3).

Further, the formability in terms of maximum peak load, surface strain, and thickness distribution obtained from FE simulation was compared with experimental data. Figure 5(b) represents the maximum peak load for different forming conditions. It was found that at $500°C$ when the deformation speed changed from 30mm/sec to 0.3mm/sec, the peak load decreased from 3.09 ton to 3 ton showing a decrement of 2.9%. In a similar manner, the decrease in load was approximately 3.5% at $650°C$. Apart from punch speed, the temperature also played a crucial role in the deformation. The maximum punch load decreased by around 5.1% (30mm/sec) and 6% (0.3mm/sec) when the temperature was increased from $500°C$ to $650°C$. This observation signifies that the effect of deformation speed on peak load becomes more pronounced at a higher temperature. Further, the FE predicted result showed that the peak

load was closer to experimental result at a reference temperature (500°C) and punch speed (30mm/sec) with an error of 2.2%. The variation was found to increase with an increase in temperature and decrease in deformation speed. However, the variation of the predicted load was found to be within the error limit of 8.6%.

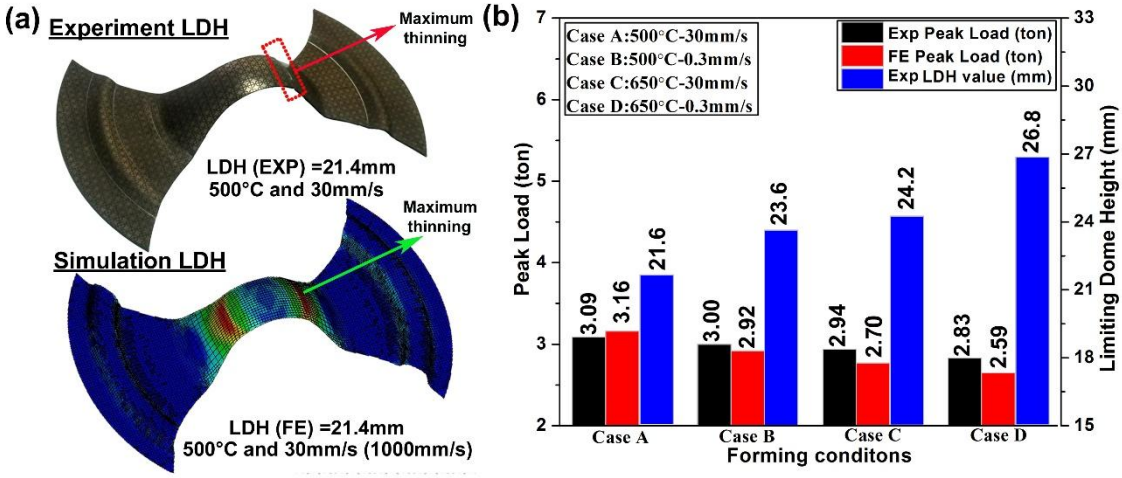

Figure 5. Experimental and FE predicted: (a) stretch formed component at similar dome height (b) peak load at different forming conditions.

For easy reference, the conditions: 500°C -30mm/s, 500°C -0.3mm/s, 650°C -30mm/s, 650°C -0.3mm/s are referred as case A, case B, case C, and case D respectively. Figure 6 depicts the evaluated thickness and true major strain distribution evaluated experimentally and compared with predicted data. For case A, the maximum thinning was around 0.79, and it increased by approximately 6.3%, 8.9%, and 12.7% for case B, case C, and case D respectively. Figure 6(b) represents true major strain distribution where the highest value of 0.83 was obtained for case D and the lowest value was found in case A with a value of 0.54. Thus, the results clearly indicate that the condition at which maximum thinning occurred led to maximum deformation in the material which was signified by the highest LDH for case D. Besides these, it is evident from the figure that both the curves showed well-developed thinning and strain distribution profile, and it was found to be increased with the increase in temperature from 500°C to 650°C and with a decrease in deformation speed from 30mm/sec to 0.3mm/sec.

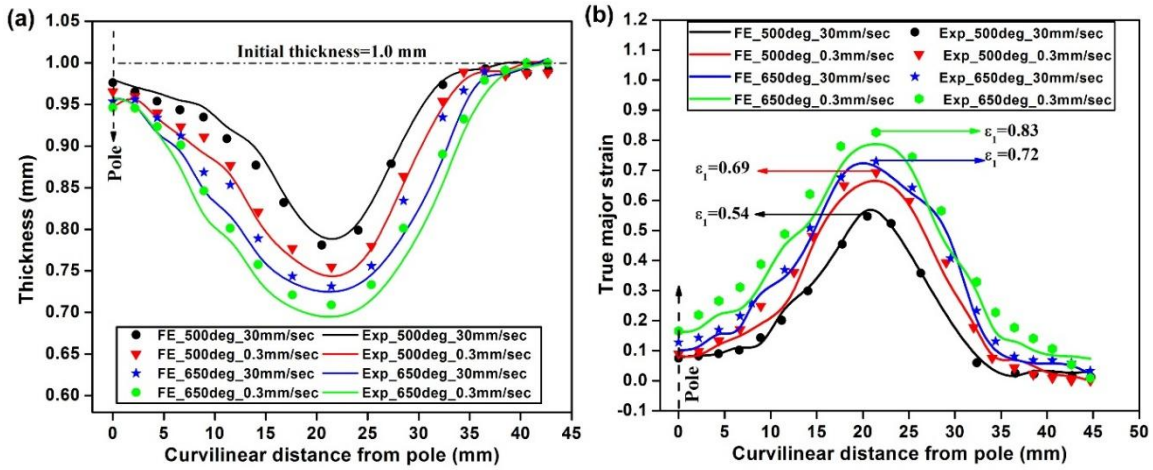

Figure 6. Experimental versus predicted (a) thickness distribution (b) true major strain distribution.

Further, it was noted that FE results fairly predicted the experimentally obtained thickness and strain profile. The data shows that it under-predicts the maximum thinning and major strain values at higher temperatures. It can be concluded that the JC model was able to capture the formability very well at

reference temperature and reference strain rate. However, the model was inadequate to provide good flow description over the entire range of temperature and deformation speed.

6. Conclusions and future scope

The main conclusions from the present work are as follows:

1. The uniaxial tensile testing within a temperature range of 500°C – 700°C at an interval of 50°C and crosshead velocities of 30, 3, 0.3, and 0.03mm/s were carried out. It was observed that the total elongation improved by approximately 18% with the increase in temperature from 500°C to 700°C. Also, a considerable reduction in total elongation with increase in flow stress was found with the increase in deformation speed at elevated temperatures.
2. Johnson-Cook model was developed successfully and its suitability was compared in term of three statistical parameters viz. the correlation coefficient (R), average absolute error (Δ), and standard deviation (SDA). It was observed that the model could predict the flow behavior with R of 0.97, and the corresponding Δ and SDA values were 10.8% and 6.8% respectively. Moreover, to validate the developed constitutive model, the predicted flow stress was successfully implemented in the coupled thermo-mechanical FE codes.
3. Formability measures such as peak punch load, thickness distribution, and strain distribution were compared between the experimental and predicted data. The results confirmed that JC model could able to capture the deformation behavior consistently with peak punch load within error of 8.6%. Also, it is noteworthy that the model could able to track the exact deformation behavior at a reference temperature and reference deformation speed.

Future scope of the present work is to develop the physical based constitutive models such as MTS and ZA in order to check the flow stress predictability over the entire testing conditions. Also, the investigation of fracture surface will be done to comprehend the deformation mechanism.

Acknowledgements

The authors thank Indian Space Research Organization (ISRO), Government of India, through KCSTC, IIT Kharagpur (IIT/KCSTC/CHAIR./NEW.APPR./13-14/64) for the financial support.

References

[1] Prasad K S, Panda S K, Kar S K, Sen M, Murty S N and Sharma S C 2017 *J. Mater. Eng. Perform.* ***26*****(4)** 1513-30
[2] Kumar D R and Swaminathan K 1999 *Mater. Sci. Technol.* **15(11)** 1241–52
[3] Toros S, Ozturk F and Kacar I 2008 *J. Mater. Process. Technol.* **207** 1–12
[4] Ghavam K, Bagheriasl R and Worswick M J 2013 *J. Manuf. Sci. Eng.* **136** 11006
[5] Xiao J, Li D S, Li X Q and Deng T S 2012 *J. Alloys Compd.* **541** 346–52
[6] Prasad K S, Gupta A K, Singh Y and Singh S K 2016 *J. Mater. Eng. Perform.* **25(12)**, 5411- 23
[7] Lin Y C and Chen X-M 2011 *Mater. Des.* **32** 1733–59
[8] Oliveira D A, Worswick M J, Finn M and Newman D 2005 *J. Mater. Process. Technol.* **170** 350–62
[9] Panicker S S, Prasad K S, Basak S and Panda S K 2017 *J. Mater. Eng. Perform.* **26** 3954–69
[10] Ozel T, Llanos I, Soriano J and Arrazola P J 2011 *Mach. Sci. Technol.* **15** 21–46
[11] Sue J A and Chang T P 1995 *Surf. Coatings Technol.* **76** 61–69
[12] Abedrabbo N, Pourboghrat F and Carsley J 2006 *Int. J. Plast.* **22** 342–73
[13] Gu S, McCartney D G, Eastwick C N and Simmons K 2004 *J. Therm. Spray Technol.* **13** 200– 13
[14] Thakur D G, Ramamoorthy B and Vijayaraghavan L 2009 *Mater. Des.* **30** 1718–25
[15] Hosaeus H, Seifter A, Kaschnitz E and Pottlacher G 2001 *High Temp. Press.* **33** 405–10